

Persistence to high temperatures of interlayer coherence in an organic superconductor

John Singleton¹, PA G oddard^{1,2}, A Ardavan², A I Coldea³, S J Blundell², R D McDonald¹, S Tozer⁴, JA Schlueter⁵¹National High Magnetic Field Laboratory, MPA-NHMF L, TA-35,

M S-E 536, Los Alamos National Laboratory, Los Alamos, NM 87545, USA

²Department of Physics, University of Oxford, The Clarendon Laboratory, Parks Road, Oxford OX1 3PU, UK³H. H. Wills Physics Laboratory, Bristol University, Tyndall Avenue, Bristol, BS9 1TL, UK⁴NHMF L, 1800 E. Paul Dirac Drive, Tallahassee FL 32310, USA⁵Materials Science Division, Argonne National Laboratory, Argonne, Illinois 60439, USA

(Dated: March 23, 2024)

The interlayer magnetoresistance R_{zz} of the organic metal $-(\text{BEDT-TTF})_2\text{Cu}(\text{NCS})_2$ is studied in fields of up to 45 T and at temperatures T from 0.5 K to 30 K. The peak in R_{zz} seen in in-plane fields, a definitive signature of interlayer coherence, remains to T s exceeding the Anderson criterion for incoherent transport by a factor ~ 30 . Angle-dependent magnetoresistance oscillations are modeled using an approach based on field-induced quasiparticle paths on a 3D Fermi surface, to yield the T dependence of the scattering rate τ^{-1} . The results suggest that τ^{-1} does not vary strongly over the Fermi surface, and that it has a T^2 dependence due to electron-electron scattering.

PACS numbers: 74.70.Kn, 71.20.Rv, 78.20.Ls

The past two decades have seen a tremendous blossoming of interest in compounds that possess quasi-two-dimensional (Q2D) electronic bandstructure; examples include crystalline organic metals [1, 2, 3, 4], cuprates [5] and layered ruthenates [6]. These materials may be described by a tight-binding Hamiltonian in which the ratio of the interlayer transfer integral t_z to the average intralayer transfer integral t_{ij} is $\ll 1$ [1, 2, 3, 4]. The question arises as to whether the interlayer charge transfer is coherent or incoherent in these materials, i.e. whether or not the Fermi surface (FS) is three dimensional (3D), extending in the interlayer direction. Various criteria for interlayer incoherence have been proposed, including [7]

$$k_B T > t_z; \quad (1)$$

where T is the temperature. In this picture, thermal fluctuations "wipe out" details of the interlayer periodicity [7]. The consequent interlayer incoherence is used as a justification for a number of theories which are thought to be pivotal in the understanding of Q2D materials (see e.g. [7, 8, 9, 10]). It is therefore important to test assertions such as Eq. 1. To this end, we have measured the magnetic-field-orientation dependence of the resistance of the organic metal $-(\text{BEDT-TTF})_2\text{Cu}(\text{NCS})_2$ [9] using fields of up to 45 T and T s of up to 30 K (Fig. 1). This material was chosen because its FS is well known [9, 11] (see Fig. 2(c)), previous low- T experiments have shown that the interlayer transfer integral is $t_a = 0.065 \pm 0.007$ meV [11, 12] and modest T s allow the inequality in Eq. 1 to be exceeded by orders of magnitude ($t_a = k_B T \approx 0.5$ K). Our data show that interlayer coherence survives to at least $k_B T > 30t_a$ (c.f. Eq. 1). In addition, the results in this paper determine the low- T scattering rate τ^{-1} for the quasiparticles. Recent works stress that an understanding of the effects of the scattering mechanism in organic metals gives vital information about the mechanism for superconductivity [13, 14].

Electrical contacts were made to single crystals (

$0.7 \times 0.5 \times 0.1$ mm³) of $-(\text{BEDT-TTF})_2\text{Cu}(\text{NCS})_2$ using 12.5 μm Pt wire bonded by graphite paste; contact resistances were $\sim 10 \Omega$. Current and voltage terminals were arranged such that the measured resistance R_{zz} is proportional to the interlayer component of the resistivity tensor, ρ_{zz} [11]. The measurements in Figs. 1 and 2 use a well-characterized crystal also employed in Refs. [4, 11, 15]. Additional experiments (e.g. Fig. 3) used d8- $-(\text{BEDT-TTF})_2\text{Cu}(\text{NCS})_2$ crystals; here, "d8" indicates that the terminal hydrogens of BEDT-TTF have been replaced by deuterium. These crystals were studied in Ref. [11], where it was found that deuteration reduces t_a to 0.045 ± 0.005 meV. Samples were mounted on a ceramic holder attached to a cryogenic goniometer allowing continuous rotation in static magnetic fields B . Crystal orientations are labeled by the angles θ ; ϕ . Here, θ is the angle between B and the normal to the highly-conducting planes and ϕ defines the plane of rotation; $\phi = 0$ is a plane of rotation containing the k_b direction and the normal to the highly-conducting planes [11]. Samples were stabilized using a calibrated Cemox sensor mounted on the sample holder and a heater driven by a feedback circuit. The Cemox resistance was monitored during isothermal field sweeps in order to deduce the correction to the apparent T due to magnetoresistance; results were in good agreement with the study of Ref. [16]. Static fields were provided by the 45 T Hybrid magnet at NHMF L Tallahassee and 33 T Bitter magnets at Tallahassee and HFM L Nijmegen.

Typical R_{zz} data are shown in Figs. 1(a) ($\theta = 160^\circ$) and 1(b) ($\theta = 90^\circ$) for T s in the range 5.3 K to 29.3 K. In the former rotation plane, features in R_{zz} are known to be due to orbits on the Q1D FS sections [11], whereas in the latter they can be confidently attributed to Q2D FS orbits [11]. A series of angle-dependent magnetoresistance oscillations (AMROs), periodic in $\tan \theta$ [9, 11] is observed at both θ ; those due to the Q2D FS sections are frequently known as Yamaji oscillations [9]. In addition,

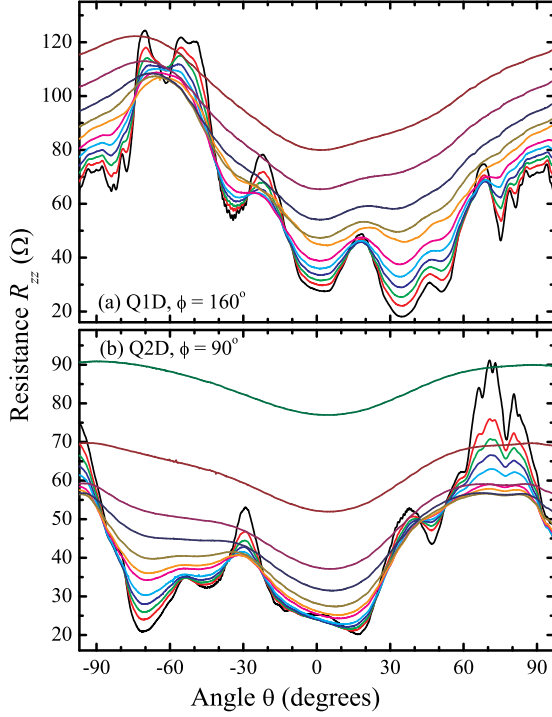


FIG. 1: Interlayer resistance R_{zz} (Ω) of a $-(\text{BEDT-TTF})_2\text{Cu}(\text{NCS})_2$ crystal versus tilt angle θ for various constant T ; $B = 45 \text{ T}$. (a) Data for $\phi = 160^\circ$, a plane of rotation at which R_{zz} is determined by phenomena on the Q1D FS sections. In order of increasing R_{zz} at $\theta = 35^\circ$, the curves are for $T = 5.3, 6.5, 7.6, 8.6, 9.6, 10.6, 12.1, 13.1, 14.6, 17.1, 19.6$ and 29.3 K respectively. In addition to AMROs, DKCOs can be seen as twin peaks on either side of $\theta = 90^\circ$ in the lower T data. (b) Similar data for $\phi = 90^\circ$; here R_{zz} features are associated with the Q2D FS section. In order of increasing R_{zz} at $\theta = 70^\circ$, the curves are for $T = 5.3, 7.6, 8.6, 9.6, 10.6, 12.1, 13.1, 14.6, 17.1, 19.6, 24.5$ and 29.3 K respectively.

Danner-Kang and Chaikin oscillations (DKCOs) [11, 17] are observed as peaks either side of $\theta = 90^\circ$ when $\phi = 160^\circ$. As T increases, the AMROs decrease in intensity, with the higher-index oscillations (i.e. those closer to $\theta = 90^\circ$ [11]) disappearing first. After most AMROs disappear, the slowly-varying background magnetoresistance begins to increase more markedly.

Figures 2(a) and (b) show expansions of data in Fig. 1 close to $\theta = 90^\circ$ at selected T s. For ease of comparison, data are plotted as $\Delta\rho_{zz} = \rho_{zz}/\rho_{zzBG}$, the fractional deviation in ρ_{zz} from the background magnetoresistance ρ_{zzBG} determined by fitting a smoothly-varying curve through the data on either side of $\theta = 90^\circ$ [4]. In such measurements, interlayer coherence is detected using a phenomenon known as the "coherence peak" or "SQUIT" (Suppression of Quasiparticle Interlayer Transport) peak [1, 2, 4, 9, 11], a maximum in $\rho_{zz} = \rho_{zzBG}$ observed when B lies exactly in the intralayer plane (i.e. at $\theta = 90^\circ$). This occurs because of the efficient interlayer velocity averaging caused by closed orbits on the side of the FS (Fig. 2(c-e)); these can exist if, and only if [1, 4], the interlayer transport is coherent, i.e. the FS is

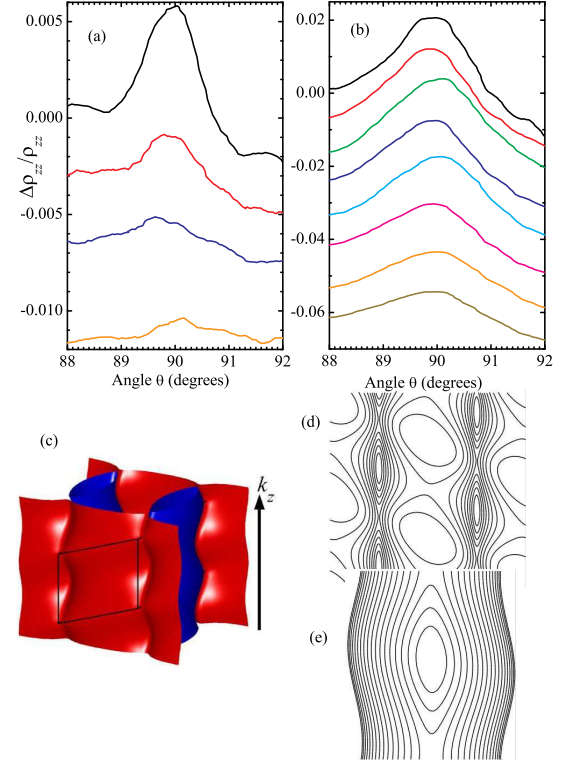


FIG. 2: (a) The 45 T magnetoresistance close to $\theta = 90^\circ$ at $\phi = 160^\circ$, plotted as $\rho_{zz} = \rho_{zzBG}$, the fractional change in ρ_{zz} from the more slowly-varying background. Data for $T = 5.3$ (highest), $7.6, 9.6$ and 13.1 K (lowest) are shown, offset for visibility. (b) Similar data for $\phi = 90^\circ$; the traces are for $T = 5.3$ (highest), $7.6, 8.6, 9.6, 10.6, 12.1, 13.1$ and 14.6 K (lowest). Each trace has been offset for clarity. (c) 3D representation of the FS of $-(\text{BEDT-TTF})_2\text{Cu}(\text{NCS})_2$ (after Ref. [11]); the finite t_a gives the corrugations (shown greatly exaggerated) on the sides of the FS. Q1D and Q2D FS sections are shown in red and blue respectively. (d) Consequent field-induced closed orbits on the side of the Q1D FS section when $\theta = 90^\circ$ and $\phi = 0^\circ$. (e) Similar closed orbits on the Q2D FS section when $\theta = 90^\circ$ and $\phi = 90^\circ$. Orbits such as those in (d) and (e) give rise to the SQUIT peak in ρ_{zz} .

a 3D entity extending in the interlayer direction. In both Figs. 2(a) and (b), the SQUIT peak is visible close to $\theta = 90^\circ$. In spite of the small size of t_a , this demonstration of interlayer coherence continues to be observable up to at least 14.6 K , exceeding the criterion in Eq. 1 by a factor ~ 30 [18].

The AMROs and DKCOs in Fig. 1 are very similar to those observed at $T = 0.5 \text{ K}$ [11], the only difference being that they decrease in amplitude as T increases; i.e. the magnetoresistance features do not change in form or angular position as T grows, they merely fade gradually. This suggests that the same mechanism is responsible for the form of the magnetoresistance at all T examined. Moreover, the SQUIT peak (Fig. 2) demonstrates that the FS of $-(\text{BEDT-TTF})_2\text{Cu}(\text{NCS})_2$ remains 3D up to at least $T \sim 15 \text{ K}$ [18]. We therefore choose to simulate the data using the numerical method based on field-

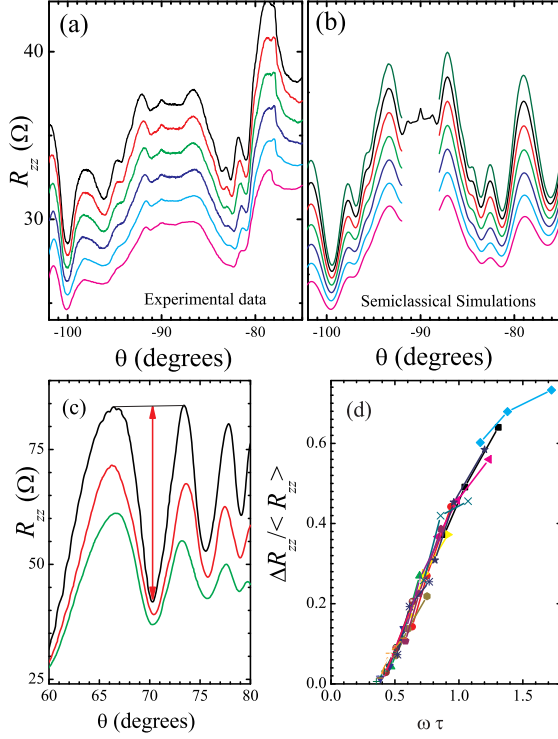


FIG. 3: Comparison of experimental $_{zz}$ data (a) and the numerical simulation (b) method described in Ref. [11]. $T = 1.5$ K and $\phi = 15^\circ$; for the lowest to the highest traces, B is 32, 34, 36, 38, 40, 42 and 44 T (no offset is applied). (c) AMRO data for $\phi = 150^\circ$, $T = 1.5$ K and fields of 20 (lowest), 24 and 28 T (highest). The arrow indicates the amplitude R_{zz} of a particular AMRO feature; $\langle R_{zz} \rangle$ is the resistance at the arrow's midpoint. (d) Experimental AMRO $R_{zz} = \langle R_{zz} \rangle$ for $\phi = 150^\circ$ plotted as a function of the orbit angular frequency ω times scattering time τ . Data for several AMROs, denoted by their Yamaji indices [9] i are shown ($i = 2$ (square), $i = 3$ (dot), $i = 4$ (triangle) and $i = 5$ (inverted triangle)) for several T s in the range 1.7 K to 5.5 K.

induced quasiparticle trajectories across a 3D FS that was used to model $T = 0.5$ K AMRO results successfully in Ref. [11]. This procedure employs Chambers' Equation and the experimentally-deduced FS (Fig. 2(c) [11]); given B and the angles ϕ , the only input parameter required to calculate $_{zz}$ is τ . The model has the restriction that magnetic breakdown between the Q1D and Q2D FS sections [20] is not included; recently it was shown that breakdown in $-(\text{BEDT-TTF})_2\text{Cu}(\text{NCS})_2$ can produce a series of AMROs [21]. However, the breakdown amplitude falls off rapidly with increasing B [20], so that these effects are small for $B \leq 45$ T when $\phi > 70^\circ$ [21]. In the following, we neglect data at lower B for this reason.

A typical comparison of experiment and simulation is shown in Figs. 3(a) and (b) ($\phi = 15^\circ$). For each B , it is possible to map the normalized AMRO amplitude

$R_{zz} = \langle R_{zz} \rangle$ (see Fig. 3(c)) from the simulation onto the experimental value by adjusting τ . Moreover, for each T , it was found that the same τ , to within experimental errors, fitted all the AMRO features. Given this

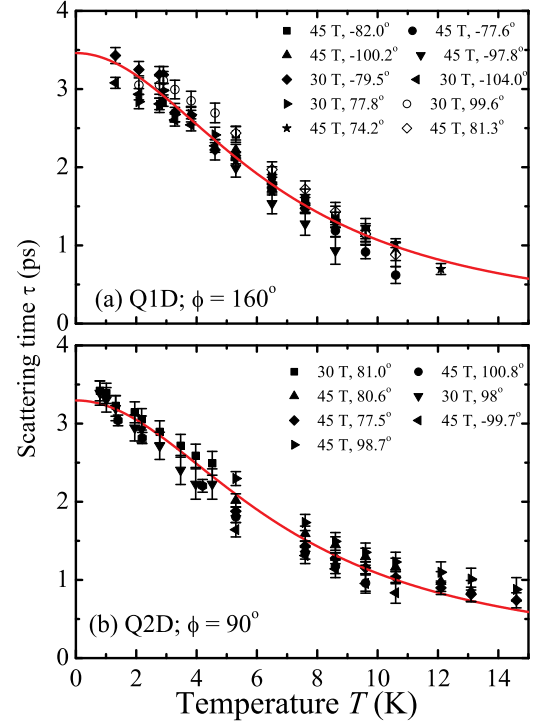


FIG. 4: Scattering time τ deduced from AMROs at 160° (a) and 90° (b) versus T . Consistent values of τ are deduced from several AMRO features at fields of 30 T and 45 T (insets show field and ϕ for each feature). The data are fitted to $\tau = (\tau_0^{-1} + AT^2)^{-1}$ (curves) with $\tau_0 = 3.3 \pm 0.1$ ps and $A = 0.0062 \pm 0.0003 \text{ ps}^{-1} \text{ K}^{-2}$ (a) and $\tau_0 = 3.5 \pm 0.1$ ps and $A = 0.0065 \pm 0.0003 \text{ ps}^{-1} \text{ K}^{-2}$ (b). These scattering rates are identical to within experimental errors, even though the AMROs in (a) and (b) are produced by different FS sections.

result, it is useful to find a single parameter to describe all AMRO amplitudes for a particular ϕ . A good candidate is τ , where τ is the angular frequency at which the orbit responsible for the AMRO feature is traversed. In the case of AMROs due to the Q2D FS sections, $\tau = (eB/m) \cos \phi$, the cyclotron frequency [11]. Here, m is the $m = 0$ effective mass of the Q2D pocket of the Fermi surface [9, 20]. For orbits on the Q1D Fermi surface, the relevant period is the time to cross the Brillouin zone [22]. As long as one avoids the region close to $\phi = 90^\circ$ where the SQUIT and DKCOs occur (the latter involving orbits that "snake" across contours on the FS [11, 17]), this frequency can be expressed as $\tau = (2eB/(m - m_{\text{eff}})) \cos \phi$, where m is the $m = 0$ effective mass of the "snake" breakdown orbit [20].

Using these τ s, the $R_{zz} = \langle R_{zz} \rangle$ values of all of the AMRO features at a particular ϕ collapse onto a single curve as a function of τ ; an example is shown in Fig. 3(d) for Yamaji oscillations due to the Q2D FS. Once this correspondence is known for each ϕ , τ can be readily found from AMRO data. The τ values thus obtained follow a T -dependence of the form $\tau^{-1} = \tau_0^{-1} + AT^2$ rather closely. Moreover, to within experimental errors, the scattering rates have the same τ_0 and values of A ,

irrespective of the FS orbits involved. This is illustrated in Fig. 4, which shows ρ_{xx} deduced from AMROs at $\mu = 160$ (a)–due to Q1D FS sections) and $\mu = 90$ (b)–due to Q2D FS sections). In spite of the fact that the quasiparticle orbits involved are very different, and involve distinct FS sections, the T dependence of ρ_{xx} for both is virtually identical. This suggests that mechanisms for superconductivity in organic metals that involve a large variation in scattering rate over the FS (e.g. \textit{FLEX} methods [23]) are inappropriate for ρ_{xx} in $\text{-(BEDT-TTF)}_2\text{Cu(NCS)}_2$. For all FS orbits studied, the inferred $T = 0$ scattering time ($\tau_0 = 3.4 \pm 0.2$ ps–see Fig. 4) is close to values measured by other means [15].

The T^2 dependence of ρ_{xx} suggests electron-electron scattering [24]. A T^2 scattering rate was inferred from $B = 0$ resistivity measurements [25]. However, problems in deconvolving the in-plane resistivity component ρ_{xx} from ρ_{zz} in experimental data [9, 15], and the influence of the broad superconducting transition on the T -dependence of the measured resistivity [9] mean that this attribution can not be considered conclusive. By contrast, the T -dependent AMROs provide an unambiguous gauge of the scattering rate of normal-state quasiparticles, allowing the mechanism to be definitively identified.

When $k_B T > 4t_a$, the interlayer contribution to the bandwidth, the FS shown in Fig. 2(c) is “blurred” on a wavevector scale $k_B T \sim v_F$ (where v_F is the Fermi velocity) exceeding the amplitude of interlayer corrugation. Nevertheless, a Fermi-liquid picture predicts that the semiclassical dynamics of each electron are still governed by an equation of motion which contains and reflects the detailed nature of the interlayer dispersion. Quasiparticle states within $k_B T$ of the chemical potential continue to contribute to the AMROs and SQUIT, as long as the underlying dispersion is not affected by a variation in

electron energy on the scale of $k_B T$; this will hold when $k_B T \ll t_{jj} \approx 10 \text{--} 100 \text{ meV}$ [11]. Then, the only effect of raising T is from T -dependent contributions to the scattering rate. This is exactly what we find in our AMRO data, and demonstrates that a coherent 3D FS picture is valid for this compound, at least at $T < 0.1t_{jj}$ (a limit our experiments do not exceed), at which point a crossover to an incoherent regime might be expected [26].

In summary, the orientation dependence of the interlayer magnetoresistance ρ_{zz} of $\text{-(BEDT-TTF)}_2\text{Cu(NCS)}_2$ has been studied in fields of up to 45 T as a function of temperature T . The “SQUIT” or coherence peak in ρ_{zz} seen in exactly in-plane fields, a definitive signature of a 3D Fermi surface (i.e. interlayer coherence), persists to temperatures exceeding the proposed Anderson criterion for incoherent transport (Eq. 1 [7]) by a factor ≈ 30 . Features in the magnetoresistance have been successfully modelled using an approach based on field-induced quasiparticle paths on a 3D Fermi surface, to yield the temperature dependence of the quasiparticle scattering rate. The results suggest that the average scattering rate does not vary strongly over the Fermi surface, and that it follows a T^2 dependence attributable to electron-electron scattering.

This work is funded by US Department of Energy (DOE) LDRD grants 20040326ER and 20030084DR and by EPSRC (UK). NHMFL is supported by the National Science Foundation, DOE and the State of Florida, and HFM L Nijmegen by EuroMagNET (EU contract RII3-CT-2004-506239). Work at Argonne was supported by the Office of Basic Energy Sciences, US DOE (contract W-31-109-ENG-38). PAG and AA acknowledge support from the Glasstone Foundation and the Royal Society respectively. Neil Harrison, Ross McKenzie and Nic Shannon are thanked for helpful discussions.

-
- [1] R.H. McKenzie and P. Monaghan, *Phys. Rev. Lett.* **81**, 4492 (1998).
 - [2] T. Otsada et al., *Physica E* **18**, 200 (2003).
 - [3] A.G. Lebed et al., *Phys. Rev. Lett.* **93**, 157006 (2004).
 - [4] J. Singleton et al., *Phys. Rev. Lett.* **88**, 037001 (2002).
 - [5] N.E. Hussey *J. Phys. Chem. Solids*, **67**, 227 (2006).
 - [6] E. Rzepniewski et al., *J. Phys.: Condens. Matter*, **14**, 3759 (2002).
 - [7] The theory of superconductivity in the high T_c cuprates, P.W. Anderson (Princeton University Press, 1997), p. 50.
 - [8] D.G. Clarke and S.P. Strong, *Adv. Phys.* **46**, 545 (1997); *J. Phys.: Condens. Matter* **8**, 5415 (1996).
 - [9] J. Singleton and C.H. Mielke, *Contemp Phys.* **43**, 63 (2002).
 - [10] N. Shannon et al., *Phys. Rev. B* **55**, 12963 (1997).
 - [11] P.A. Goddard et al., *Phys. Rev. B* **69**, 174509 (2004).
 - [12] $\text{-(BEDT-TTF)}_2\text{Cu(NCS)}_2$ ’s monoclinic structure means that the interlayer transfer integral is along the a axis, i.e. not normal to the conducting planes [11]. Hence, it is labeled t_a rather than t_z .
 - [13] B.J. Powell and R.H. McKenzie, *Phys. Rev. B* **69**, 024519 (2004).
 - [14] J.G. Analytis et al., *Phys. Rev. Lett.* **96**, 177002 (2006).
 - [15] J. Singleton et al., *J. Phys: Condens. Matter*, **15**, L203 (2003).
 - [16] B.L. Brandt et al. *Rev. Sci. Instr.* **70**, 104 (1999).
 - [17] G.M. Danner et al., *Phys. Rev. Lett.* **72**, 3714 (1994).
 - [18] In fact the data show that some vestiges of a 3D FS persist up to at least 50 K [19].
 - [19] P.A. Goddard et al., preprint (2006).
 - [20] N. Harrison et al. *J. Phys.: Condens. Matter* **8**, 5415 (1996).
 - [21] A. Bangura et al., preprint (2006).
 - [22] A. Ardavan et al., *Phys. Rev. Lett.* **81**, R6129 (1997).
 - [23] K. Kuroki et al., *Phys. Rev. B* **65**, R100516 (2002); J. Schmalian, *Phys. Rev. Lett.* **81**, 4232 (1998).
 - [24] *Solid State Physics*, by N.W. Ashcroft, N.D. Mermin (Holt-Saunders, New York, 1976), p. 347.
 - [25] *Organic Superconductors* by T. Ishiguro, K. Yamaji and G. Saito (Springer-Verlag, Berlin 1998).
 - [26] J. Merino and R.H. McKenzie, *Phys. Rev. B* **61**, 7996 (2000).